A pervaporation model : Membrane design

Tyagi, R. K.; Fouda, A. E.; Matsuura, T.

Publisher's version / Version de l'éditeur:
https://doi.org/10.1016/0009-2509(95)00148-X
Chemical Engineering Science, 50, 19, pp. 3105-3114, 1995-10

Pergamon

Chemical Engineering Science, Vol. 50, No. 19, pp. 3105–3114, 1995

0009–2509/95 $9.50 + 0.00

0009–2509(95)00148–4

A PERVAPORATION MODEL: MEMBRANE DESIGN

R. K. TYAGI, A. E. FOUDA† and T. MATSUURA*
Institute for Environmental Research and Technology, National Research Council, Ottawa, Canada K1A 0R6

(*First received* 9 *December* 1994; *revised manuscript received and accepted* 24 *April* 1995)

Abstract—Theoretical penetrant concentration profiles under steady-state pervaporation conditions were generated using a newly developed transport model. The transport model assumes the presence of an imaginary phase (liquid or vapor) which is in thermodynamic equilibrium with the membrane phase. Theoretical profiles were compared with experimental concentration profiles. The calculation for the phase boundary between imaginary liquid and vapor phases was also performed using the transport model. The present work is the first theoretical work that can reconstruct penetrant profiles inside the membrane showing concentration polarization.

INTRODUCTION

Pervaporation transport is commonly described by a solution-diffusion model (Greenlaw *et al.*, 1977; Mulder *et al.*, 1985; Neel, 1991), free volume model (Huang *et al.*, 1992) or a pore-flow model (Okada and Matsuura, 1991). The solution-diffusion model does not consider phase boundary inside the membrane, while the pore-flow model does. As early as 1961, Binning *et al.* (1961) considered this phase change within the membrane.

Although there are some studies concerning penetrant profiles inside the membrane (Kim and Kammermeyer, 1970; Mulder *et al.*, 1985) a systematic study for binary mixtures has not been done. A comprehensive study was undertaken to obtain experimental penetrant profiles inside the membrane under steady-state pervaporation condition (Tyagi *et al.*, 1992; Tyagi, 1993; Tyagi and Matsuura, 1994).

A transport model was developed to describe mass transport during steady-state pervaporation (Tyagi *et al.*, 1994). The mathematical equations obtained for pure penetrant permeation are the same as those derived by the pore-flow model (Okada and Matsuura, 1991). Based on the analysis of a binary mixture system, the possibility of a concentration polarization phenomenon occurring inside the membrane was pointed out. In the analysis of the binary mixture system, coupling was considered in the liquid-transport region of the membrane but no coupling was considered in the vapor-transport region of the membrane. The theoretical prediction of concentration polarization occurring inside the membrane was substantiated by experimental data (Tyagi *et al.*, 1992; Tyagi and Matsuura, 1995).

In the present study an attempt has been made to compare experimental penetrant profile data with theoretical profiles.

THEORETICAL DEVELOPMENT

The salient features of the newly developed transport model are that it:

- Assumes the presence of an imaginary phase (liquid or vapor) in equilibrium with the membrane phase.
- Considers the phase change of penetrant(s) in the imaginary phase.
- Considers the pressure profile inside the membrane.
- Utilizes experimental sorption data from liquid and vapor phases.
- Assumes an isothermal condition across the membrane.
- Considers coupling in the liquid-transport region of the membrane but does not consider coupling in the vapor-transport region of the membrane.

The chemical potential gradient is considered to be the driving force for the flow of the penetrant. A membrane is split along the penetrant flow direction into small segments and the presence of an imaginary liquid (or vapor) phase which is in thermodynamic equilibrium with each membrane segment is assumed. A schematic diagram is shown in Fig. 1. The first membrane segment is in sorption equilibrium with the feed liquid. Accordingly an imaginary phase is in sorption equilibrium with the penetrant in each segment. Such an imaginary phase should be liquid when the segment is closer to the liquid feed side. As one moves in the direction of penetrant flow, the pressure and the composition of the imaginary liquid phase should change gradually. At a point, where vapor

*Present address: IMRI, Department of Chemical Engineering, University of Ottawa, Ottawa, Canada K1N 6N5.
† Corresponding author.
NRCC No. 37593.

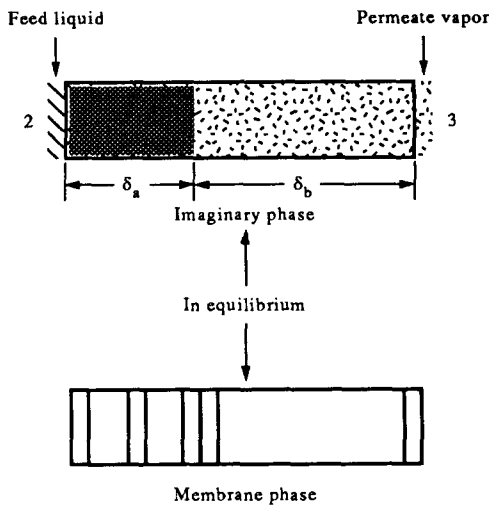

Fig. 1. A schematic diagram of the transport model.

pressure of the imaginary phase is no longer greater than the vapor pressure of the penetrant, the imaginary phase would be in the vapor state. Therefore, as far as the imaginary phase is concerned, there exists a clear boundary between the liquid and vapor phases. Adsorption equilibrium is established between the imaginary vapor phase and the penetrant in the membrane. When the transport takes place in the part of the membrane that is in equilibrium with the imaginary liquid phase, the transport is called hereafter liquid transport. When the transport takes place in the part of the membrane that is in equilibrium with the imaginary vapor phase, the transport is hereafter called vapor transport.

Since the membrane phase is in equilibrium with the imaginary phase, μ_i(imaginary phase) = μ_i (membrane phase) and a_i(imaginary phase) = a_i(membrane phase).

Mathematical equations were developed for pure component permeation. These equations resulted in the same as those developed using the pore-flow model (Okada and Matsuura, 1991). For binary mixture permeation, the theory concludes the possibility of the presence of concentration polarization occurring inside the membrane. Experimental evidence of concentration polarization was presented in an earlier communication (Tyagi and Mastuura, 1995).

STRATEGY FOR PLOTTING THEORETICAL CONCENTRATION PROFILES INSIDE THE MEMBRANE FOR BINARY MIXTURE SYSTEMS

Using the new transport model (Tyagi *et al.*, 1994), the theoretical concentration profile of the slower component (acetic acid in this case) can be plotted by following the method described in this section.

Calculation of the phase boundary in the imaginary phase at a fixed temperature

The transport equation for pure component permeation was developed in an earlier communication (Tyagi *et al.*, 1994). The final mathematical expression is as follows:

$$J = \frac{A}{\delta}(P_2 - P_*) + \frac{B}{\delta}(P_*^2 - P_3^2) \tag{1}$$

where A (mol/s m^2 Pa) and B (mol/s m^2 Pa^2) denote liquid- and vapor-transport parameters involving several physical quantities. P_2, P_*, P_3 and δ are upstream pressure (Pa), saturated vapor pressure at the phase boundary (Pa), downstream pressure (Pa) and total membrane thickness (m), respectively.

If liquid-transport and vapor-transport regions are denoted by δ_a and δ_b, the transport equation for the pure component for vapor penetration rate can be written as follows:

$$J = \frac{B}{\delta_b}(P_*^2 - P_3^2). \tag{2}$$

Therefore, vapor permeation rate equations for components i and j can be written as follows:

$$J_i = \frac{B_i}{\delta_b}(P_{i,*}^2 - P_{i,3}^2) \tag{3}$$

$$J_j = \frac{B_j}{\delta_b}(P_{j,*}^2 - P_{j,3}^2). \tag{4}$$

The variables used in the above equations are defined in the notation section. Subscripts $*$ and 3 refer to the phase boundary and the downstream side, respectively.

Rearranging eqs (3) and (4) yields

$$J_i = \frac{B_i}{(\delta)(\delta_b/\delta)}(P_{i,*}^2 - P_{i,3}^2) \tag{5}$$

$$J_j = \frac{B_j}{(\delta)(\delta_b/\delta)}(P_{j,*}^2 - P_{j,3}^2). \tag{6}$$

Furthermore, the following equation is valid:

$$\frac{\delta_a}{\delta} + \frac{\delta_b}{\delta} = 1. \tag{7}$$

Among the variables involved in the above equations, the known quantities are:

- (B_i/δ) and (B_j/δ) at 25°C which can be obtained from the permeation data of pure component for the ith and jth component, respectively.
- J_i, J_j, $P_{i,3}$ and $P_{j,3}$, which are available from the steady-state pervaporation experiments of the binary mixture.

Equations (5)–(7) can be solved by using the vapor–liquid equilibrium data and following the iteration method to calculate the position of the phase boundary (δ_a/δ and δ_b/δ). Iterations are performed by using the values of $P_{i,*}$ and $P_{j,*}$ from vapor–liquid equilibrium data. Here $P_{i,*}$ and $P_{j,*}$ indicate the partial vapor pressures of components i and j, respectively. Initial (guess) values of $P_{i,*}$ and $P_{j,*}$ are to be taken from vapor–liquid equilibrium data. Therefore, the values of δ_a/δ and δ_b/δ and the best-fit values of

$P_{i,*}$ and $P_{j,*}$ can be obtained using eqs (5)–(7) by the iteration method and using the vapor–liquid equilibrium data. Vapor–liquid equilibrium data for the acetic acid–water system at different temperatures were taken from the literature (Gmehling *et al.*, 1981).

From the vapor–liquid equilibrium data of components i and j the following relationships can be written:

$$P_{i,*} + P_{j,*} = P_* \tag{8}$$

where P_* is the total vapor pressure. Also,

$$Y_{i,*} = \frac{P_{i,*}}{P_*} \tag{9}$$

$$Y_{i,*} = f(X_{i,*}) \tag{10}$$

where $Y_{i,*}$ and $X_{i,*}$ are the mole fractions of component i at phase boundary in the vapor phase, and liquid phase, respectively. Using eqs (8)–(10) the values of $Y_{i,*}$ and $X_{i,*}$ corresponding to the best-fit values of $P_{i,*}$ and $P_{j,*}$ can be obtained. These values will be used in the next section to calculate the mass transfer coefficient.

Calculation of mass transfer coefficient

The equation for concentration polarization based on the boundary film theory approach can be written as follows:

$$\frac{X_{i,*} - Y_{i,3}}{X_{i,2} - Y_{i,3}} = \exp(v/k) \tag{11}$$

where $X_{i,2}$, $X_{i,*}$ and $Y_{i,3}$ are the mole fractions of component i in the liquid feed mixture, at phase boundary, and in the downstream, respectively. In eq. (11), v and k represent penetrant velocity (m/s) and mass transfer coefficient (m/s) in the imaginary phase, respectively. A general derivation of the concentration polarization equation based on boundary film theory can be found in standard membrane text-books, e.g. Matsuura (1994). In the present case it is assumed that component i (acetic acid) permeates through the membrane more slowly than component j and the thickness of the liquid-filled region is equal to the thickness of the boundary layer. The above equation is derived to describe the phenomenon of concentration polarization occurring inside the membrane. At steady state, the net flow rate of component i in the liquid-filled region is the sum of the diffusive flow and the convective flow and should be equal to the permeation rate of component i through the membrane.

Furthermore, the following relationship is valid:

$$v = M_{\text{mix}}(J_i + J_j)/\rho_{\text{mix}} \tag{12}$$

where v, M_{mix} and ρ_{mix} are penetrant velocity (m/s), molecular weight of the mixture (kg/mol) and density of the mixture (kg/m^3), respectively. Equation (12) can be rearranged to give the following expression:

$$v = \frac{J_i M_i}{\rho_i} + \frac{J_j M_j}{\rho_j} \tag{13}$$

where ρ_i, ρ_j, M_i and M_j are density of penetrant i, density of penetrant j (kg/m^3), molecular weight of component i and j, respectively. It is assumed that densities of the ith and jth components (ρ_i and ρ_j) in the mixture are the same as their pure component densities. Quantities J_i and J_j are known from pervaporation data. Therefore, the value of v can be calculated from eq. (13) by substituting the values of known parameters on the right side. The derivation of eq. (13) is shown in Appendix A.

In eq. (11) the following quantities are known:

- $X_{i,*}$ from eqs (8)–(10).
- $Y_{i,3}$ and $X_{i,2}$ from pervaporation data.

The value of the mass transfer coefficient in the imaginary phase, k, can be calculated from eq. (11) by substituting the known quantities and the value of v obtained from eq. (13).

Calculation of phase boundary and mass transfer coefficient at different temperatures

The values of parameters B_i/δ and B_j/δ at 25°C were used to perform the calculations. These values were obtained from pure component permeation data at 25°C. For the permeation data of the pure components (water and acetic acid) the permeation rate for each component was recorded against the downstream pressure. These parameters were calculated in an earlier communication (Tyagi *et al.*, 1994). It should be noted that these parameters will change with temperature. Pure component permeation data are available only at 25°C. The parameters at 35 and 40°C were obtained in the following manner.

From eq. (3) the permeation rate equations for component i at 25 and 35°C can be written as

$$J_{i,25} = \frac{B_{i,25}}{\delta_{b,25}}(P^2_{i,*,25} - P^2_{i,3,25}) \tag{14}$$

and

$$J_{i,35} = \frac{B_{i,35}}{\delta_{b,35}}(P^2_{i,*,35} - P^2_{i,3,35}). \tag{15}$$

The first subscript in the sequence of subscripts, i.e. i or j, refers to component i or j. The second subscript $*$ or 3 refers to the vapor–liquid equilibrium boundary or to the downstream, respectively. The third subscript 25 or 35 refers to the temperature of the feed mixture in °C. Therefore, in this case $P_{i,*,25}$ indicates the saturation vapor pressure of component i at 25°C and $B_{i,25}$ refers to the parameter B for component i at 25°C. By rearranging eqs (14) and (15), the following expression can be obtained:

$$\frac{B_{i,35}}{\delta_{b,35}} = \frac{B_{i,25}}{\delta_{b,25}} \times \frac{J_{i,35}}{J_{i,25}} \times \frac{P^2_{i,*,25} - P^2_{i,3,25}}{P^2_{i,*,35} - P^2_{i,3,35}}. \tag{16}$$

A similar relationship can be obtained for component j:

$$\frac{B_{j,35}}{\delta_{b,35}} = \frac{B_{j,25}}{\delta_{b,25}} \times \frac{J_{j,35}}{J_{j,25}} \times \frac{P^2_{j,*,25} - P^2_{j,3,25}}{P^2_{j,*,35} - P^2_{j,3,35}}. \tag{17}$$

In the above equations the values of $P_{i,*,35}$ and $P_{j,*,35}$ for the desired composition can be obtained from vapor–liquid equilibrium data. The values of parameters $J_{i,25}$, $J_{j,35}$, $P_{i,3,25}$ and $P_{j,3,35}$ (corresponding to the downstream pressure conditions) can be obtained from the pervaporation data. Thus, the numerical value of the parameter $B_{i,35}/\delta_b$ can be calculated if the value of the parameter $B_{i,25}/\delta_b$ is known with one single pervaporation data at 35°C. Similarly the values of the parameter B/δ_b at 40°C can be computed for both components separately by a single pervaporation data at 40°C.

Penetrant profile in the imaginary phase

The objective now is to generate the penetrant composition profile along the penetrant flow direction in the liquid-transport and in the vapor-transport regions of the membrane. At this point it should be remembered that we are still dealing with the imaginary phase and not the membrane phase. For the case when the imaginary phase is liquid, the following equation can be used to find different $X_{i,l}$ (refers to the value of X_i at any position l) values at different positions (l) in the membrane:

$$\frac{X_{i,l} - Y_{i,3}}{X_{i,2} - Y_{i,3}} = \exp\left(\frac{v}{k} \times \frac{l}{\delta_a}\right). \tag{18}$$

This equation can also be derived from the boundary film theory and will give us the values of $X_{i,l}$ at different positions, i.e. l/δ_a. This relative distance should be converted to l/δ, which is relative to the total membrane thickness.

Equations (3) and (4) can be rewritten in the following manner for calculating the vapor pressure at a position l_v from the phase boundary inside the membrane along the penetrant flow direction:

$$J_i = \frac{B_i}{(\delta)(l_v/\delta)}(P_{i,*}^2 - P_{i,l}^2) \tag{19}$$

$$J_j = \frac{B_j}{(\delta)(l_v/\delta)}(P_{j,*}^2 - P_{j,l}^2). \tag{20}$$

A further rearrangement of eqs (19) and (20) leads to the following equations for the calculation of partial vapor pressures of components i and j:

$$P_{i,l} = \sqrt{P_{i,*}^2 - J_i \times \frac{(l_v/\delta)}{(B_i/\delta)}} \tag{21}$$

$$P_{j,l} = \sqrt{P_{j,*}^2 - J_j \times \frac{(l_v/\delta)}{(B_j/\delta)}}. \tag{22}$$

These equations will give the value of $P_{i,l}$ and $P_{j,l}$ and, therefore, the mole fraction of component i can be calculated as follows:

$$Y_{i,l} = P_{i,l}/(P_{i,l} + P_{j,l}).$$

The position l_v/δ should be converted to relative distance l/δ measured relative to the membrane–feed mixture interface. By combining the data for the liquid and vapor regions, the composition data (mole fraction of acetic acid in this case) of the imaginary phase at different positions across the membrane can be obtained.

Penetrant profile in the membrane phase

As the presence of an imaginary phase in equilibrium with the membrane phase is assumed, sorption (liquid or vapor) data are to be used to generate the penetrant profile in the membrane phase. In other words, the sorption data are applied to find the composition of the penetrant in the membrane phase using that of the imaginary phase. When the imaginary phase is liquid, corresponding penetrant amount and composition of the membrane phase is obtained from the liquid sorption data. Similarly, when the imaginary phase is vapor, vapor sorption data are used to obtain the penetrant amount and composition in the membrane phase.

Therefore, for the slower component (acetic acid) the following two family of curves (in membrane phase) can be obtained:

- Mole fraction of acetic acid in the membrane phase vs the relative distance in the membrane.
- Total penetrant (sorbed) amount in the membrane phase vs the relative distance in the membrane.

These profiles obtained from the transport model are to be compared with the experimental penetrant concentration profiles. Experimental profiles were obtained using a stack of identical membranes during steady-state pervaporation.

Assuming convective flow for liquid mixtures in the liquid-transport portion of the membrane, the equation for A_{mix} for the liquid mixture can be written as follows:

$$J_i + J_j = \frac{A_{mix}}{\delta_a}(P_2 - P_*). \tag{23}$$

It should be noted that a strong coupling, and no separation, is assumed in liquid transport, whereas no coupling is considered in vapor transport. The possibility of convective flow for liquid mixtures is documented in the literature (Adam *et al.*, 1983).

EXPERIMENTAL

A stack of dense aromatic polyamide films was used to generate experimental data on penetrant profile studies. An acetic acid–water system was used. These experiments were performed by using a stack of identical membranes during steady-state pervaporation, stopping the pervaporation experiment, dividing the stack into substacks, then desorbing and analyzing the penetrants from each substack (Tyagi *et al.*, 1994; Tyagi and Matsuura, 1995). Sorption experiments were performed from liquid phase and vapor phase for the same binary mixture of acetic acid and water. The sorption experiments from the liquid phase were performed at 25, 35 and 40°C over the entire binary

mixture composition range. Vapor sorption isotherms were also established at these temperatures (Tyagi, 1993). In the present paper these sorption data will be used only for prediction purpose.

RESULTS AND DISCUSSIONS

Testing the transport model

The newly developed transport model was used to calculate the theoretical penetrant concentration profile curves. The following data are needed to generate these curves:

- Vapor–liquid equilibrium data for the acetic acid–water system at 25, 35 and 40°C.
- Pure component permeation data at different downstream pressures to obtain B_i/δ and B_j/δ parameters. These parameters were calculated using the pure component permeation data of individual components at a fixed temperature.
- Liquid and vapor sorption data for the binary system for the same polymeric membrane at 25, 35 and 40°C. The sorption data are necessary to find the sorbed amount and the mole fraction of each component in the membrane phase in equilibrium with the imaginary phase. In the present paper sorption data will be used to generate penetrant profiles only. Detailed sorption data will be presented in a later communication.

Effect of process variables on the phase boundary

The effect of different process variables on the phase boundary was calculated using the newly developed transport model. The summary of calculation results is shown in Tables 1, 2 and 3.

The effect of downstream pressure on the liquid–vapor phase boundary is shown in Table 1. This table shows the results for the phase boundary calculations at a feed temperature of 25°C and an acetic acid feed mole fraction of 0.50. For the downstream pressure of 467 Pa (3.5 mmHg) the vapor-transport region has the highest value. As the downstream pressure increases from 467 Pa (3.5 mmHg) to 2666 Pa (20 mmHg) the fraction of the vapor-transport region decreases from 0.85 to 0.26. As separation occurs in the vapor-transport region, the decrease in the amount of the vapor-transport fraction denotes a decrease in selectivity. This observation is in agreement with pervaporation data at these downstream pressures. In pervaporation experiments the lowest selectivity was observed for the highest downstream pressure (Tyagi *et al.*, 1994). At a downstream pressure of 2666 Pa (20.0 mmHg), the membrane was mostly filled with liquid: the relative liquid-transport region was 0.74. Since the total saturation vapor pressure of the mixture is very close to 2666 Pa (20.0 mmHg) at this temperature, it is quite reasonable to expect that the phase was mostly liquid. Thus, the transport model can describe the experimental data very well. The pervaporation mode having liquid on both sides is similar to the case in reverse osmosis in the sense that both feed and downstream are in liquid phase. The transport mechanism in pervaporation mode having liquid on both sides should be the same as in reverse osmosis.

The effect of feed composition on the vapor–liquid phase boundary is shown in Table 2. These data correspond to a downstream pressure of 467 Pa (3.5 mmHg) and a feed temperature of 25°C. A definite trend in the value of the relative vapor-transport portion can be seen when the acetic acid mole fraction is increased from 0.13 to 0.50. The relative vapor-transport portion increases from 0.51 to 0.85. In other words, the membrane selectivity should increase as the mole fraction of acetic acid is increased or the water mole fraction is decreased. Referring back to the pervaporation data of the binary mixture at the same process conditions, it is evident that the lower mole fraction of water in the binary mixture led to higher separation factors (Tyagi *et al.*, 1994). Therefore, the observed trend of the pervaporation data is in agreement with the prediction using the transport model. However, once the feed concentration of acetic acid increases further, the relative vapor-transport region diminishes to 0.72.

The effect of feed temperature on the phase boundary is shown in Table 3. These data correspond to a downstream pressure of 467 Pa (3.5 mmHg) and an

Table 1. Effect of downstream pressure on the phase boundary

Downstream pressure Pa (mmHg)	Relative liquid-transport region (δ_a/δ)	Relative vapor-transport region (δ_b/δ)
467 (3.5)	0.15	0.85
1200 (9.0)	0.22	0.78
2666 (20.0)	0.74	0.26

Table 2. Effect of feed composition on the phase boundary

Mole fraction of acetic acid in feed	Relative liquid-transport region (δ_a/δ)	Relative vapor-transport region (δ_b/δ)
0.13	0.49	0.51
0.25	0.48	0.52
0.37	0.44	0.56
0.50	0.15	0.85
0.65	0.28	0.72

Table 3. Effect of feed temperature on the phase boundary

Feed temperature (°C)	Relative liquid-transport region (δ_a/δ)	Relative vapor-transport region (δ_b/δ)
25	0.15	0.85
35	0.21	0.79
40	0.14	0.86

acetic acid mole fraction of 0.50 in the feed. The relative vapor-transport portions corresponding to the feed temperature of 25 and 40°C are similar: 0.85 and 0.86, respectively. During the steady-state pervaporation experiments, the selectivity at 25 and 40°C was the same, which can be explained by the same phase boundary position in both cases. At the feed temperature of 35°C, the vapor-transport fraction was the smallest, i.e. 0.79. Recall that concentration polarization inside the membrane was observed only at 35°C (Tyagi *et al.*, 1994). Thus, a moderate selectivity occurring inside the membrane was attributed to one of the factors leading to concentration polarization.

Table 4 is a summary of the data generated using the transport model. The table shows the acetic acid mole fraction at different positions inside the membrane. Relative mass transfer coefficients are also presented with the mass transfer coefficient at the downstream pressure of 467 Pa (3.5 mmHg), feed temperature of 25°C and at the acetic acid mole fraction of 0.50 as the basis. The absolute value of the mass transfer coefficient corresponding to the above process conditions is 6.24×10^{-8} m/s. The mass transfer coefficient at the downstream pressure of 2666 Pa (20.0 mmHg) is nearly zero. This pressure is close to the total saturation vapor pressure of the feed mixture at these conditions.

The penetrant concentration profile inside the membrane was predicted using the newly developed transport model. The prediction was made using the vapor–liquid equilibrium data, pure component permeation data, liquid sorption data, vapor sorption data and the binary mixture pervaporation data. The prediction using the transport model was compared to the experimental penetrant concentration profile. Six representative figures are shown in this paper. Both experimental and predicted penetrant concentration profiles corresponding to the same process conditions are plotted on the same figure. Figures 2, 3 and 4 show the total sorbed amount of the penetrants in the membrane phase plotted against the relative distance inside the membrane. Figure 2 corresponds to a downstream pressure of 467 Pa (3.5 mmHg), feed temperature of 25°C and acetic acid mole fraction of 0.5 in the feed mixture. Figure 3 shows the results of a downstream pressure of 467 Pa (3.5 mmHg), feed temperature of 25°C and acetic acid mole fraction of 0.25 in the feed mixture. Figure 4 shows similar data at 35°C (downstream pressure of 467 Pa and acetic acid mole fraction in the feed solution of 0.50).

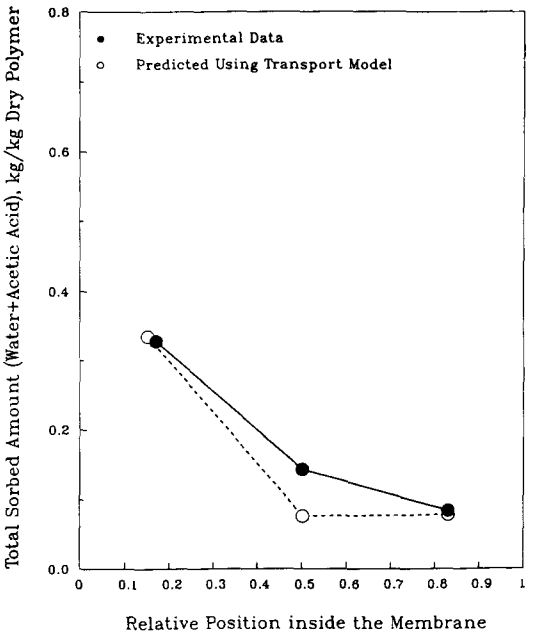

Fig. 2. Calculated penetrant profile compared with the experimental data of the acetic acid–water system at 25°C, downstream pressure = 467 Pa, AA = 0.50.

In these figures, only three data points are shown. Each experimental data point represents an average data for the corresponding section. Experimental data points were obtained using a stack of membranes. The stack was divided into three substacks and desorbed

Table 4. Summary of calculation data showing acetic acid mole fraction in the membrane phase at different positions

		Mole fraction of acetic acid					
Downstream pressure (Pa)	Temperature (°C)	in bulk solution	at feed–liquid membrane interface	at liquid–vapor boundary (liquid–transport) region	at liquid–vapor boundary (vapor–transport) region	in downstream	Relative mass transfer coefficient
467	25	0.50	0.16	0.19	0.05	0.07	1.00
1200	25	0.50	0.16	0.17	0.04	0.10	1.39
2666	25	0.50	0.16	0.16	0.03	0.12	—
467	25	0.13	0.09	0.15	0.03	0.07	0.22
467	25	0.25	0.12	0.17	0.04	0.07	0.30
467	25	0.37	0.14	0.17	0.04	0.07	0.65
467	25	0.65	0.24	0.27	0.06	0.07	1.49
467	35	0.50	0.16	0.17	0.04	0.07	1.58
467	40	0.50	0.17	0.17	0.05	0.07	3.62

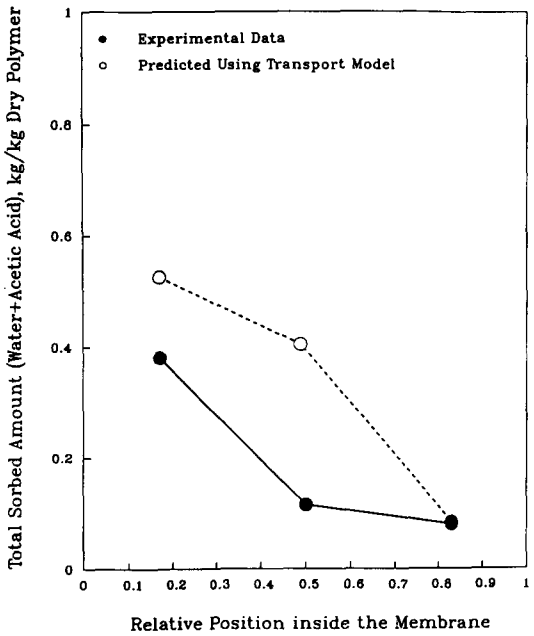

Fig. 3. Calculated penetrant profile compared with the experimental data of the acetic acid–water system at 25°C, downstream pressure = 467 Pa, AA = 0.25.

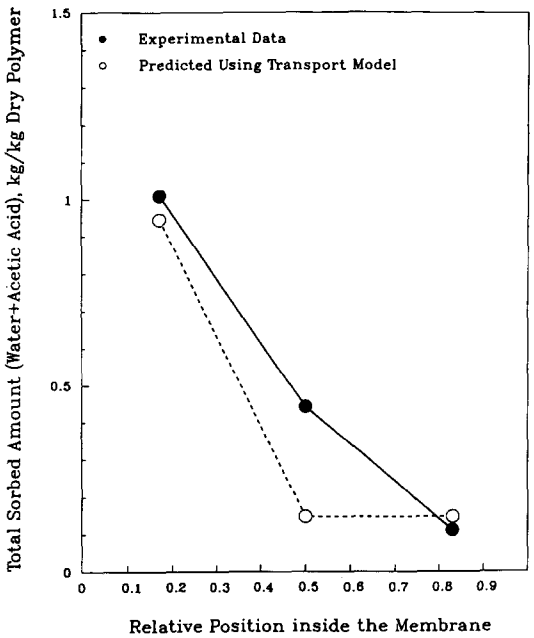

Fig. 4. Calculated penetrant profile compared with the experimental data of the acetic acid–water system at 35°C, downstream pressure = 467 Pa, AA = 0.25.

penetrant was analyzed. Calculated data points corresponding to only three relative distances inside the membrane are shown in these figures.

In all three figures, the total sorbed amount is the highest in the section in contact with the upstream liquid feed and is the least in the section in contact with the downstream permeate vapor. This change in total sorbed penetrant amount reflects the large difference in the sorbed amount depending on whether the membrane is in equilibrium with liquid or vapor phase. The amount sorbed from the liquid phase was an order of magnitude higher than that from the vapor phase (Tyagi, 1993). Agreement between the experimental and predicted data is quite good in Figs 2 and 4.

Figures 5, 6 and 7 show the calculated and experimental results for acetic acid mole fraction profile. The mole fraction is plotted against the relative distance inside the membrane in these figures. There are three experimental points available. Figure 5 shows the data at the downstream pressure of 467 Pa (3.5 mmHg) and at the feed temperature of 25°C.

In Fig. 6 a definite trend can be observed for acetic acid mole fraction inside the membrane. A maximum was observed in experiments under steady-state pervaporation conditions. In Fig. 6 the experimental acetic acid mole fraction was the highest in the middle section/substack of the membrane stack. Aromatic polyamide membranes permeate water preferentially. Therefore, acetic acid will be expected to accumulate close to the selective layer. In the present model the selective layer is the vapor-filled region. The higher mole fraction of acetic acid in the middle layer is the manifestation of this effect. The effect has close similarity to the concentration polarization phenomenon observed in reverse osmosis. The possibility of the presence of concentration polarization inside the membrane was predicted using the newly developed transport model (Tyagi and Matsuura, 1995). The predicted mole fraction of acetic acid inside the mem-

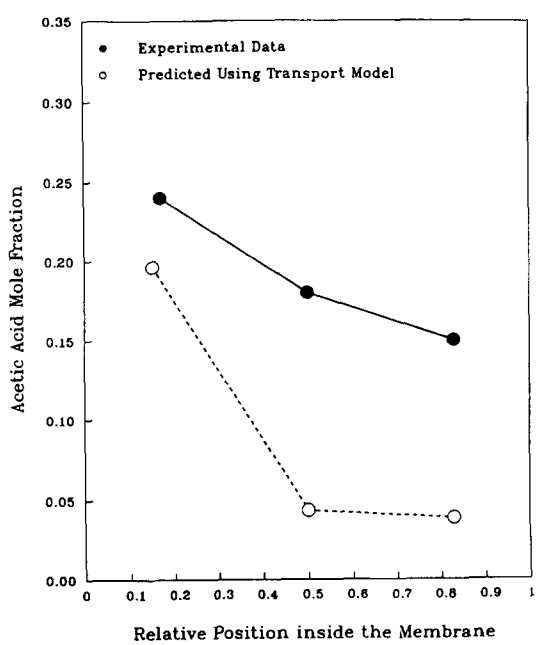

Fig. 5. Calculated penetrant profile compared with the experimental data of the acetic acid–water system at 25°C, downstream pressure = 467 Pa, AA = 0.50.

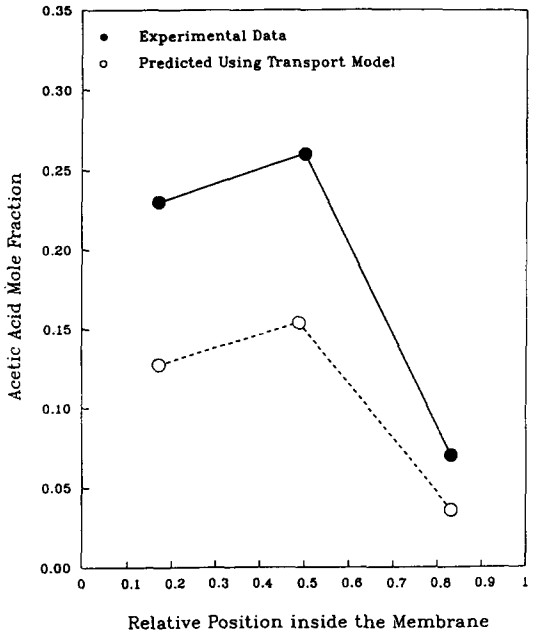

Fig. 6. Calculated penetrant profile compared with the experimental data of the acetic acid–water system at 25°C, downstream pressure = 467 Pa, AA = 0.25.

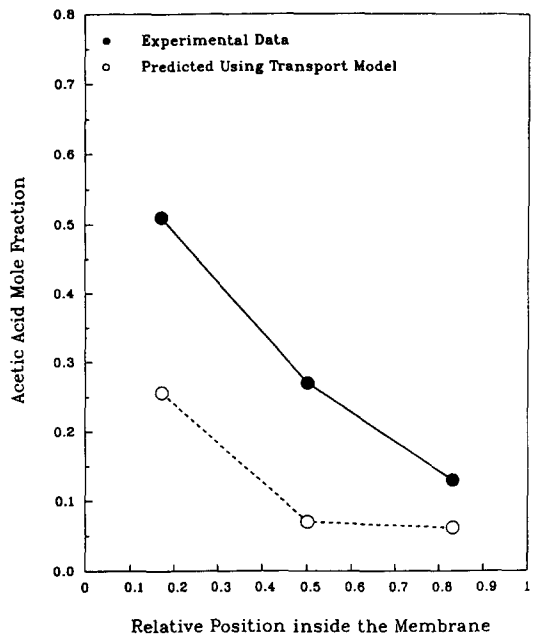

Fig. 7. Calculated penetrant profile compared with the experimental data of the acetic acid–water system at 25°C, downstream pressure = 467 Pa, AA = 0.65.

brane also shows a similar trend. Therefore, the transport model is able to describe the qualitative behavior of experimental data quite well.

Figure 7 also shows acetic acid mole fraction in the membrane phase. Experimental mole fraction in the section closest to the liquid feed is very close to the bulk feed mole fraction of the same. The mole fraction of acetic acid in the section closest to the downstream side is close to the mole fraction in permeate. In this figure also, the transport model can reproduce the qualitative behavior of the experimental data.

It should be recalled that the coupling between the flow of two penetrants (acetic acid and water in this case) was considered in the liquid-transport section of the membrane. The coupling was not considered in the vapor-transport section of the membrane. If the coupling phenomenon in the vapor-transport region is also quantified and incorporated into the transport model, the agreement with the experimental data would be even better. Incorporating coupling parameters will also explain membrane selectivity decrease at higher acetic acid concentrations as extent of coupling changes with feed composition. On the other hand, the transport model would become more complex as compared to the present simple and easy-to-use model.

It should also be pointed out that the phenomenon of concentration polarization occurring inside the membrane was first reported in the present work. Other transport models available in the literature fail to predict this phenomenon. Therefore, the present work is the first theoretical work that can reconstruct the penetrant concentration profiles inside the membrane showing concentration polarization. The present work is also the first attempt to examine the predictability of the newly developed transport model.

The uniqueness of concentration polarization phenomenon occurring only at a certain temperature (e.g. at 35°C) can be explained qualitatively in terms of penetrant–penetrant interaction, penetrant–polymer interaction and the plasticizing effects of the penetrants. Acetic acid forms dimers and can also associate with water in the solution. Water can also form clusters in the membrane. All of the equilibrium constants associated with these effects will change with temperature and composition of the mixture, and the presence of the polymeric membrane will further complicate the case. The decoupling of these effects is not possible at this stage. The simultaneous presence of these effects makes the profile data at a particular temperature and feed composition unique data for a particular membrane–penetrants system.

IMPLICATIONS OF THE EXPERIMENTAL DATA FOR THE MEMBRANE DESIGN

In the present study a transport model was used which considers a phase boundary between the imaginary liquid and vapor phases. The imaginary phase is in thermodynamic equilibrium with the membrane phase. It was assumed that the part filled with liquid is nonselective and the part filled with vapor is selective. Based on these assumptions an analysis of the binary mixture permeation led to the possibility of the concentration polarization occurring inside the membrane. This theoretical prediction was substantiated with the help of experimental data obtained. The

phenomenon of concentration polarization occurred in some specific cases but not in all cases.

The typical concentration polarization equation involves the term $\exp(v/k)$, which represents concentration polarization modulus. This term should be minimized in order to minimize the concentration polarization phenomenon. In the above expression v is defined by eq. (13) and is the penetrant permeation velocity. The mass transfer coefficient (D/δ_a) is denoted by k. Here D represents the diffusion coefficient of penetrant in the liquid-transport region and δ_a is the interfacial boundary layer thickness or the thickness of the liquid-transport layer.

There are two possibilities to minimize this term. The first one is to lower v, which is impractical since an increase in v is normally desirable. The other possibility is to maximize k, i.e. maximize the mass transfer coefficient. Mass transfer can be maximized by either

- reducing the thickness of the liquid-transport region, or
- increasing the value of the diffusion coefficient D.

In the present case, the interfacial layer represents the liquid-transport region of the pore or the layer where liquid transport takes place. For pervaporation, the diffusivity of the penetrant inside the membrane is a function of the penetrant concentration in the membrane. A high concentration of the penetrant inside the membrane results in a greater value of diffusivity.

From all pervaporation data obtained it was quite clear that the permeation rate was greater when the concentration of the penetrant inside the membrane was greater in the liquid-transport portion of the membrane. For example, for the pure water permeation case, the highest permeation flux (1.62×10^{-3} mol/s m^2) was observed while the sorbed amount of the penetrant in the liquid-transport region (the section in contact with liquid feed) was also the highest (0.718 kg/kg of dry polymer). Therefore, higher penetrant concentration in the membrane will lead to a greater diffusivity value, greater mass transfer coefficient, and eventually, to greater total permeation rates.

Thus, minimization of concentration polarization is favorable to obtain greater permeation rates and lower concentration polarization modulus. In conclusion, concentration polarization occurring inside the membrane has negative side effects, e.g. lower permeation rate and lower selectivity.

A novel composite pervaporation membrane can be designed based on the above observations. This membrane should utilize a bottom layer for selectivity; hence it should be a dense and selective layer. The top layer should have good interaction with the preferentially permeating component. A dense polymeric base film (to achieve high selectivity) should, therefore, be coated with a thin layer of hydrophilic polymer for the purpose of preferential permeation of water from a water–acetic acid mixture. In order to achieve high permeation rates the base membrane should not be very dense otherwise the permeation rate will be sacrificed. The top layer should also be as thin as possible. The following requirements must be satisfied for the design of composite membranes:

(1) The thickness of the layer, where the liquid transport takes place, should be as thin as possible to increase the mass transfer coefficient of the layer.
(2) The coated layer should be as highly swollen as possible to increase the penetrant diffusivity.
(3) The bottom layer, where the vapor transport takes place, should be dense so that a high selectivity can be achieved. The thickness of this vapor transport layer should be controlled to achieve an optimized flux.

CONCLUSIONS

- The newly developed transport model can describe the qualitative behavior of the experimental data. Therefore, the present work is the first theoretical work that can reconstruct penetrant profiles inside the membrane showing concentration polarization.
- The concentration polarization occurring in the membrane should be minimized. The minimization of this phenomenon is favorable to obtain grater permeation rates during steady-state pervaporation. Concentration polarization modulus can be minimized by
  - keeping the liquid-transport region δ_a/δ as small as possible,
  - keeping penetrant concentration of the preferentially permeating component in the liquid-transport region of the membrane as high as possible.

A novel membrane design for pervaporation separation has been proposed. This membrane is a composite membrane consisting of two distinct layers. The top layer should be as thin as possible. The top part of the polymeric membrane should have strong interaction with the preferentially permeating component of the mixture. The bottom layer should be the selective layer and should be dense.

NOTATION

B_i, B_j	vapor-transport parameter for components i and j, respectively, mol/s m^2 Pa^2
J_i, J_j	permeation flux of components i and j, respectively, mol/m^2 s (kg/m^2 h)
M_i, M_j	molecular weights of components i and j, respectively, kg/mol
$P_{i,*}$, $P_{j,*}$	partial vapor pressure of components i and j, respectively, at the phase boundary, Pa (mmHg)
$P_{i,3}$, $P_{j,3}$	partial vapor pressure of components i and j, respectively, in the downstream vapor, Pa (mmHg)
k	mass transfer coefficient, m/s
v	penetrant velocity, m/s

w_i, w_j weight fraction of components i and j in the mixture, respectively

Greek letters

δ total membrane thickness, m

δ_a, δ_b liquid- and vapor-transport regions of the membrane, respectively, m

ρ_i, ρ_j density of components i and j, respectively, kg/m^3

ρ_{mix} density of mixture, kg/m^3

REFERENCES

Adam, W. J., Luke, B. and Meares, P., 1983, Mixture of organic liquid by hyperfiltration. *J. Membrane Sci.* **13**, 127–149.

Binning, R. C., Lee, R. J., Jennings, J. F. and Martin, E. C., 1961, Separation of liquid mixtures by permeation. *Ind. Engng Chem.* **53**, 45–50.

Gmehling, J., Onken, U. and Arlt, W., 1981, *Vapor–Liquid Equilibrium Data Collection: Aqueous–Organic Systems* (Suppl. 1), Chemistry Data Series, Vol. I, Part 1a. DECHEMA, Frankfurt.

Greenlaw, F. W., Prince, W. D., Shelden, R. A. and Thompson, E. V., 1977, Dependence of diffusive permeation rates on upstream and downstream pressures: I. Single component permeant. *J. Membrane Sci.* **2**, 141–151.

Huang, R. Y. M., Balakrishnan, M. and Rhim, J. W., 1992, Pervaporation separation of pentane–alcohol mixture using nylon 6–polyacrylic acid (PAA) ionically crosslinked membranes. II. Exprimental data and theoretical interpretation. *J. Appl. Polym. Sci.* **46**, 109–118.

Kim, S. N. and Kammermeyer, K., 1970, Actual concentration profiles in membrane permeation. *Sep. Sci.* **5**, 679–697.

Matsuura, T., 1994, *Synthetic Membranes and Membrane Separation Processes*, Chap. 5. CRC Press, Boca Raton.

Mulder, M. H. V., Franken, A. C. M. and Smolders, C. A., 1985, On the mechanism of separation of ethanol–water mixtures by pervaporation. II. Experimental concentration profiles. *J. Membrane Sci.* **23**, 41–58.

Neel, J., 1991, *Pervaporation Membrane Separation Processes* (Edited by R. Y. M. Huang). Elsevier, New York.

Okada, T. and Matsuura, T., 1991, A new transport model for pervaporation. *J. Membrane Sci.* **59**, 133–150.

Tyagi, R. K., 1993, Ph.D. thesis, Department of Chemical Engineering, University of Ottawa, Ottawa.

Tyagi, R. K., Fouda, A. E., Handa, P. and Matsuura, T., 1992, Transport studies in pervaporation, in *Proceedings of the 6th International Conference on Pervaporation Processes in Chemical Industry* (Edited by R. Bakish), pp. 320–334. Bakish Materials Corp., Englewood Cliffs, New Jersey.

Tyagi, R. K., Fouda, A. E. and Matsuura, T., 1994, Possibility of concentration polarization occurring inside the membrane during steady state pervaporation. *Chem. Engng Commun.* (accepted).

Tyagi, R. K. and Matsuura, T., 1995, Concentration polarization occurring inside the membrane during steady state pervaporation. *Chem. Engng Commun.* **134**, 157–170.

APPENDIX A

$$v = M_{mix}(J_i + J_j)/\rho_{mix}.$$

Let X_i and X_j be mole fractions and w_i and w_j be the weight fractions of components i and j, respectively. The following expressions can be written:

$$X_i = J_i/(J_i + J_j) \quad \text{and} \quad X_j = J_j/(J_i + J_j)$$

$$X_i + X_j = 1 \quad \text{and} \quad w_i + w_j = 1.$$

The following relationship between the mole fraction X_i and weight fraction w_i can be written:

$$w_i = M_i X_i/(M_i X_i + M_j X_j).$$

The following xpression can also be written for the mixture density:

$$1/\rho_{mix} = w_i/\rho_i + w_j/\rho_j$$

which yields

$$\rho_{mix} = \rho_i \rho_j/(w_i \rho_j + w_j \rho_i).$$

The molecular weight of the mixture can be written as follows:

$$M_{mix} = X_i M_i + X_j M_j.$$

By substituting the values of ρ_{mix}, M_{mix} and mole fractions, the following expression for the penetrant velocity can be obtained:

$$v = (J_i + J_j)(X_i M_i + X_j M_j) \times \frac{M_i X_i \rho_j/(M_i X_i + M_j X_j) + M_j X_j \rho_i/(M_i X_i + M_j X_j)}{\rho_i \rho_j}.$$

By simplifying the above expression and substituting the values of mole fraction in terms of permeation flux (J_i and J_i), the following expression can be obtained:

$$v = \frac{J_i M_i}{\rho_i} + \frac{J_i M_i}{\rho_j}.$$

The above expression is the same as eq. (13).